



**HAL**  
open science

# Augmenting road noise engineering methods using the Boundary Element Method

Matthew Kamrath, Julien Maillard, Philippe Jean, Dirk van Maercke,  
Judicaël Picaut

► **To cite this version:**

Matthew Kamrath, Julien Maillard, Philippe Jean, Dirk van Maercke, Judicaël Picaut. Augmenting road noise engineering methods using the Boundary Element Method. INTERNOISE 2016, International Congress and Exposition of Noise Control Engineering, Aug 2016, HAMBOURG, Germany. 12p. hal-01373714

**HAL Id: hal-01373714**

**<https://hal.science/hal-01373714>**

Submitted on 29 Sep 2016

**HAL** is a multi-disciplinary open access archive for the deposit and dissemination of scientific research documents, whether they are published or not. The documents may come from teaching and research institutions in France or abroad, or from public or private research centers.

L'archive ouverte pluridisciplinaire **HAL**, est destinée au dépôt et à la diffusion de documents scientifiques de niveau recherche, publiés ou non, émanant des établissements d'enseignement et de recherche français ou étrangers, des laboratoires publics ou privés.



## Augmenting road noise engineering methods using the Boundary Element Method

Matthew KAMRATH<sup>1</sup>; Julien MAILLARD<sup>2</sup>; Philippe JEAN<sup>3</sup>; Dirk VAN MAERCKE<sup>4</sup>;

Judicaël PICAUT<sup>5</sup>

<sup>1,2,3,4</sup> Building Science and Technology Center (CSTB), France

<sup>5</sup> IFSTTAR, France

### ABSTRACT

Exposure to excessive noise is correlated with higher rates of annoyance, sleep disturbance, and other negative health outcomes. Accurately calculating road noise in complex urban environments is fundamental to assessing potential noise mitigation devices and reducing overall noise exposure. However, computing sound propagation in this setting is difficult because cities have complicated geometries and large domains. For example, engineering methods such as ISO-9613-2 or NMPB 2008 efficiently estimate sound levels but cannot model complex geometries like a T-barrier. In addition, detailed approaches such as the boundary element method or the finite-difference time-domain method produce precise results for any geometry but rapidly become too expensive as the frequency and domain size increase. Using a hybrid formulation alleviates these problems. Specifically, the boundary element method yields a table of the corrections for the domain's involved structures for a range of source and receiver positions and frequencies. Interpolating this table, the engineering method adjusts the predicted sound level for each path. For complex objects, this hybrid method provides a substantial improvement at little additional cost compared to current engineering methods. This paper further explicates and evaluates this technique.

Keywords: hybrid, propagation, noise I-INCE Classification of Subjects Number(s): 76.1

## 1. INTRODUCTION

### 1.1 Topic Significance

According to the World Health Organization (1–4), noise is a public health threat. In Western Europe, noise annoys one in three people and disturbs the sleep of one in five. As a result, Europeans lose over 1 million healthy life years annually. In response, the European Parliament and Council enacted the Environmental Noise Directive (5), which states that environmental noise is “one of the main environmental problems in Europe.” According to the directive, current noise levels should be quantified via noise mapping, and action plans should be created and implemented to reduce environmental noise and to preserve quiet areas. Thus, the directive requires a method that models sound levels from cars and trains in urban areas.

### 1.2 Previous Research

Many numerical techniques predict urban, outdoor noise propagation, including engineering, geometrical, statistical, frequency-domain, time-domain, and hybrid methods, but most become inappropriate as the domain size and geometric complexity increase (see Table 1). Engineering methods like ISO 9613-2 (6), NMPB 2008 (7,8), Nord2000 (9,10), CNOSSOS (11), and HARMONOISE (12,13) are very computationally efficient approximations of reference calculations and measurements, yet they cannot model complicated geometries like a T-barrier. Geometrical

<sup>1</sup> matthew.kamrath@cstb.fr

<sup>2</sup> julien.maillard@cstb.fr

<sup>3</sup> philippe.jean@cstb.fr

<sup>4</sup> dirk.vanmaercke@cstb.fr

<sup>5</sup> judicael.picaud@ifsttar.fr

methods like beam tracing (14,15) and ray tracing (16,17) work well for simple cases that converge in only a few reflections. Nevertheless, they are inadequate because their cost rapidly increases with the reflection order and the models' assumption that surfaces are large compared to a wavelength is problematic for detailed geometries. Statistical approaches like the radiosity method (18,19) and the diffusion method (20–22) yield economical solutions for simple cases; nonetheless, as the complexity of the scene increases these methods become either inapplicable or prohibitively expensive. Frequency-domain approaches like the boundary element method (BEM) (23–27) and the equivalent source method (28–30) and time-domain approaches like the finite-difference time-domain method (31–34) and the transmission line matrix method (35–37) produce reference solutions for many cases. However, their computational burden is too great for this application because they quickly increase in cost with frequency and domain size. Hybrid methods (38–42) generally try to combine the best aspects of multiple methods, but most of the hybrid methods in the literature combine methods that are all too expensive for this application, so the result is also too costly.

| Insufficient detail | Both        | Too expensive    |
|---------------------|-------------|------------------|
| Engineering         | Geometrical | Frequency-domain |
|                     | Statistical | Time-domain      |
|                     | Hybrid      |                  |

Table 1 - Reasons other methods are inadequate for this application

### 1.3 Research Question

Numerical tools are integral to assessing current noise levels, evaluating potential noise mitigation techniques, and ultimately reducing overall noise levels. Nevertheless, most computational methods are too expensive or cannot model the necessary geometries or surfaces. Engineering methods are currently the standard way to predict noise levels in urban areas, but they inadequately model many important elements of an urban setting. Previous papers (25,43,44) calculate the influence of a lone barrier but give very little detail about how to incorporate these corrections into an engineering method in a complex setting. Therefore, the goal is to enable engineering methods to model more complicated objects in an urban setting while minimizing the additional computational cost.

## 2. APPROACH

### 2.1 Overall Method

Engineering methods calculate the transfer function between a source and a receiver. First, the method finds all of the paths between the source and receiver up to a given reflection order. Then, for each path summing several attenuation terms yields the total attenuation for that path. For example, engineering methods usually have at least the following terms:

$$A_{total} = A_{div} + A_{atm} + A_{dif} + \dots \quad (1)$$

where the terms on the right represent the attenuations due to geometric divergence, atmospheric absorption, and diffraction. The proposed method adds another attenuation term to the engineering methods that quantifies the effect of a complex object compared to a reference object.

$$A_{total} = A_{div} + A_{atm} + A_{dif} + \dots + A_{complex} \quad (2)$$

For any path that diffracts over a complex object, interpolating a precomputed table of corrections for the corresponding frequency and geometry determines the complex attenuation term. Lastly, summing all the path contributions produces the final transfer function.

### 2.2 Storing the Corrections

A large, 6D table contains the corrections. The variables (see Figure 1) are source frequency ( $f$ ) and position ( $x_s, z_s$ ), the receiver position ( $x_r, z_r$ ), and the distance between the source and the receiver that is parallel to the complex object ( $\Delta y$ ). This method only requires the relative y-position because at this stage the barrier is considered infinitely long, which greatly reduces the computational cost. If the

effects of a finite barrier are important, the engineering method would calculate it.

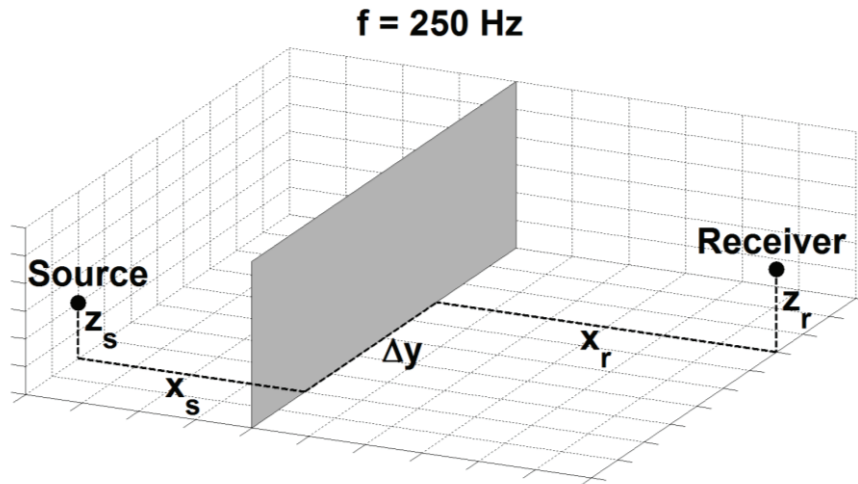


Figure 1 – The variables for storing the correction factors.

A very large, fine grid of points would provide excellent accuracy, but this option requires too much memory. The required memory grows very rapidly because there are six variables stored on a grid. For example, if there are 20 points/dimension using double precision (8 bytes/number), then the total memory would be about 0.5 GB ( $\approx 8 \times 20^6 / 1024^3$ ). For comparison, the total memory of a typical computer is only 8 GB. Thus, the maximum number of points/dimension is about twenty. Nonetheless, the range of all of the variables should be large enough to contain most (image) sources and receivers to avoid potentially inaccurate extrapolated values.

To optimize accuracy, the points are concentrated close to the barrier where the field tends to change most rapidly. For example, the results section uses the following  $\Delta y$  values (m): 0, 0.25, 0.5, 0.75, 1, 1.5, 2, 2.5, 3, 4, 5, 6, 8, 10, 12, 16, 20, 32, 48, 64, 96, and 128. This spacing is similar to log spacing, but the accuracy is significantly better with this spacing. The other variables follow a similar pattern, but the heights only go up to 10 m. This spacing is not necessarily optimal, just better than uniform or log spacing using the same number of points. Finding a better distribution of points is still an area of active research.

### 2.3 Calculating the Corrections

2.5D BEM (24) calculates the corrections using hard ground. Since the method is 2.5D, the barrier is considered infinitely long with a constant, arbitrarily-shaped cross section. BEM is advantageous in this case compared to the finite element method or the time-domain finite-difference method because BEM only meshes the perimeter of the barrier's cross section.

Each correction requires two boundary element computations, one with the complex object and one with the reference object:

$$A_{complex}(\mathbf{x}, f) = L_{complex}(\mathbf{x}, f) - L_{ref}(\mathbf{x}, f) \quad (3)$$

where  $\mathbf{x} = (x_s, z_s, x_r, z_r, \Delta y)$ . All of these corrections are stored in a .txt file, which is read by the engineering method. In this paper, this .txt file is referred to as the input file.

### 2.4 Selecting the Source and Receiver Positions

To use the table of corrections, the engineering method needs the frequency and the source and receiver positions. The frequency is given, but obtaining the source and receiver positions is more involved. If the path includes reflections from vertical surfaces or diffractions over horizontal edges, then the source and receiver positions might not be at the physical source and receiver positions from the real problem. If a reflection occurs on the source side of the complex object, then the method uses the image source; correspondingly, if the reflection is on the receiver side, then the method utilizes the image receiver. In the engineering method, this process is accomplished by first searching for paths between the source and receiver in the 2D version of the problem as seen from above. Then, the paths are unfolded so that each path is straight as seen from above. This process converts the 3D problem

into a 2D vertical slice where the coordinates are the distance along the path and the height of the path.

If multiple diffraction points are in a vertical slice (see Figure 2), then the source and receiver positions depend on the size and position of each object. To understand why, image a ray that diffracts over a very tall barrier and a relatively short barrier. This situation is similar to Figure 2 but with an even greater height disparity. In this case, the attenuation of the tall barrier is nearly unchanged by the presence of the short barrier, but the attenuation of the short barrier is greatly reduced. For the short barrier, the source appears to be at the top of the tall barrier instead of at the real source position because the sound needs to diffract over the tall barrier in order to reach the short barrier.

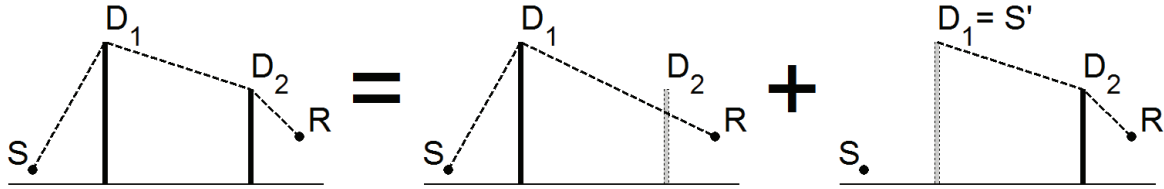


Figure 2 – The approximation for modeling multiple diffraction points

The standard way to rank the diffracting objects is by their path length differences because the attenuation is proportional to the path length difference, which is the distance from the source to the diffraction point to the receiver minus the distance from the source to the receiver (i.e.  $\Delta L_{path}(S, D, R) = d_{SDR} - d_{SR}$ ). In Figure 2,  $\Delta L_{path}(S, D_1, R) > \Delta L_{path}(S, D_2, R)$ , so the total attenuation is approximately

$$A_{total} = A(S, D_1, R) + A(D_1, D_2, R) \quad (4)$$

If  $\Delta L_{path}(S, D_1, R) < \Delta L_{path}(S, D_2, R)$ , then  $A_{total} = A(S, D_2, R) + A(S, D_1, D_2)$ . Thus, the object with the greatest path length difference sees the physical source and receiver as its source and receiver, and the other diffracting objects use either the actual source and receiver or the other diffraction points as their sources and receivers. This process can be applied to any number of diffracting objects by iteratively finding the object with the largest path length difference and using that point as the source or receiver for the remaining objects depending on if they are on the receiver or source side of the main object.

The HARMONOISE engineering method (12) models diffraction as describe above for straight barriers. The hybrid method extends this concept to complex objects and simplifies buildings, which have two diffraction points, to one diffraction point at the center of the building along the ray path. This simplification removes discontinuities in the shadow region where the largest path length difference jumps between two diffracting edges (see Figure 3).

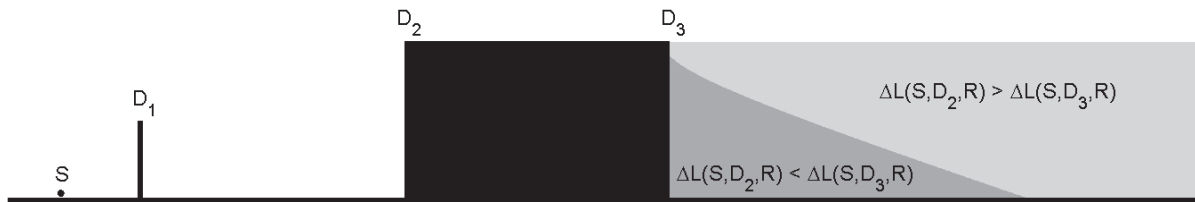


Figure 3 – A potential discontinuity if  $A(S, D_1, D_2) \neq A(S, D_1, D_3)$  that is addressed in the hybrid method

## 2.5 Interpolation

Given the frequency and source and receiver positions, a linear interpolation method yields the path's complex attenuation ( $A_{complex}$ ). First, the method finds the data points at the corners of the shape (i.e. a rectangle in 2D or a box in 3D) that contains the interpolation point. Since the data is stored on a non-uniform grid, a kd-tree produces a point's index in a time proportional to  $\log_2 N$  where  $N$  is the total number of points. Calculating the offset of the remaining points from the first point gives their indices in constant time. Next, the data positions ( $\mathbf{x}$ ) and the interpolation point ( $\mathbf{x}_{int}$ ) are converted to local coordinates between zero and one. The value at the interpolation point is

$$y(x_1, x_2, \dots, x_N) = \sum_{n_1, n_2, \dots, n_N=0}^1 c_{n_1, n_2, \dots, n_N} x_1^{n_1} x_2^{n_2} \dots x_N^{n_N} \quad (5)$$

where  $N$  is the number of dimensions,  $c_{n_1, n_2, \dots, n_N}$  is the coefficient of each of the  $2^N$  terms, and  $y$  replaces  $A_{complex}$  for brevity and generality. Since all of the subscripts are either zero or one, the entire subscript is a binary number, which arranges the coefficients in the coefficients vector, i.e.  $\mathbf{c} = [c_{0,0,\dots,0} \ c_{0,0,\dots,1} \ \dots \ c_{1,1,\dots,1}]^T$ . Evaluating the equation at each of the corners of the shape that contains the interpolation point gives  $2^N$  equations with  $2^N$  unknowns. Since the position of each data point in local coordinates is also a binary number, the values at those positions are arranged like  $\mathbf{c}$ , i.e.  $\mathbf{y} = [y(0,0, \dots, 0) \ y(0,0, \dots, 1) \ \dots \ y(1,1, \dots, 1)]^T$ . The order is important because solving this set of equations does not require a matrix inversion. In this form, the coefficients are given by the following relationships:  $\mathbf{c} = \mathbf{B}_N \mathbf{y}$ ,  $\mathbf{B}_0 = \mathbf{1}$ , and

$$\mathbf{B}_{n+1} = \begin{bmatrix} \mathbf{B}_n & \mathbf{0} \\ -\mathbf{B}_n & \mathbf{B}_n \end{bmatrix} \quad (6)$$

where  $n$  is a positive integer. Then, plugging the interpolation point into equation (5) yields the interpolated value.

To make this process concrete, consider a 2D example where the interpolation point is  $\mathbf{x}_{int} = [0.2 \ 0.3]$  and the values at the corners of the rectangle are  $\mathbf{y} = [y(0,0) \ y(0,1) \ y(1,0) \ y(1,1)]^T = [1 \ 2 \ 3 \ 4]^T$ . For a 2D problem,

$$\mathbf{B}_2 = \begin{bmatrix} 1 & 0 & 0 & 0 \\ -1 & 1 & 0 & 0 \\ -1 & 0 & 1 & 0 \\ 1 & -1 & -1 & 1 \end{bmatrix} \quad (7)$$

and

$$y(x_1, x_2) = c_{0,0} + c_{0,1}x_2 + c_{1,0}x_1 + c_{1,1}x_1x_2 \quad (8)$$

Thus,  $\mathbf{c} = [c_{0,0} \ c_{0,1} \ c_{1,0} \ c_{1,1}]^T = [1 \ 1 \ 2 \ 0]^T$  and  $y(0.2, 0.3) = 1.7$ .

## 2.6 Extrapolation

By design, most if not all of the points will be within the interpolation region; however, if a point is outside this region, then the closest point in the data table is multiplied by an extrapolation factor

$$A_{complex} = f(d)A_{complex}(\mathbf{x}_{closest}, f) \quad (9)$$

where  $d$  is the distance between the interpolation point and the data point that is closest to the interpolation point. The extrapolation factor is shown in Figure 4 and is given by the following equations:  $c_0 = 1$ ,  $c_1 = 0$ ,  $c_2 = \lambda/2.4$  where  $\lambda$  is wavelength,  $c_3 = 4/\lambda$ ,  $c_4 = c_0 + (c_0 - c_1)/(1 + e^{c_2 c_3})$ , and

$$f(d) = c_4 + \frac{c_1 - c_4}{1 + e^{-c_3(d-c_2)}} \quad (10)$$

For  $d \ll \lambda/2$ ,  $f(d) \approx 1$ ; for  $d = \lambda/2$ ,  $f(d) \approx 0.5$ ; and for  $d \gg \lambda/2$ ,  $f(d) \approx 0$ .

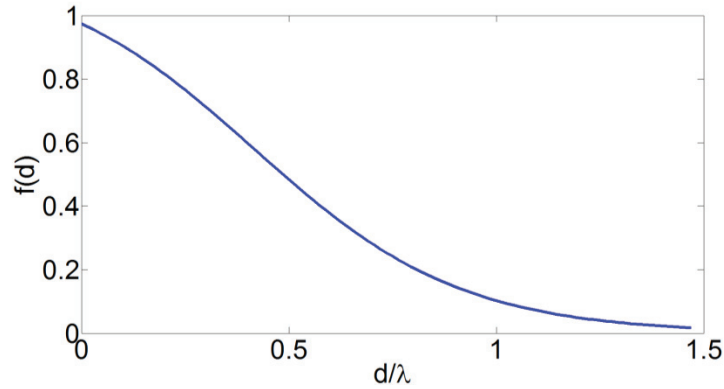


Figure 4 – The extrapolation transition region

### 3. RESULTS

#### 3.1 T-barrier

First, consider a T-barrier with a straight reference barrier (see Figure 5). This case demonstrates what information is lost due to the sparse grid spacing of the input file and the interpolation method.

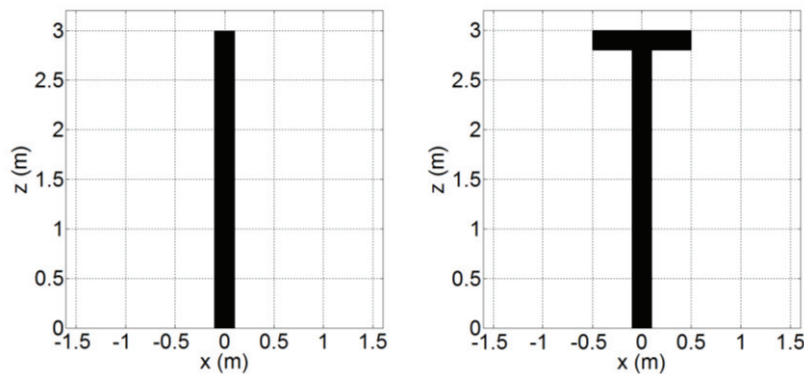


Figure 5 – The geometry of the reference (left) and complex (right) barriers. The barriers are 0.2 m thick.

The source is at  $(-3, 17.5, 0.3)$  m and the receivers are on a uniform grid at a height of 1.5 m with 25 cm spacing. The barrier is at  $x = 0$  m and is infinitely long, the ground is hard, and the frequency is the 250 Hz third-octave band. The complex attenuation term, i.e. the difference in level between the T-barrier and the straight barrier ( $A_{complex} = L_T - L_I$ ), is given in Figure 6 using BEM and in Figure 7 using the hybrid method.

Looking at Figure 6, there are a few important aspects to notice. First, the picture is symmetrical because the barrier is infinitely long, which enables the method to only need  $\Delta y$  instead of  $y_s$  and  $y_r$ . Next, previous research (43) indicates that the T-barrier is more efficient at blocking sound than a straight barrier of the same height, and these calculations tend to agree. Moreover, the correction is large compared to the typical error of an engineering method, which is about three decibels. The plot shows the majority of the area has a -7 dB correction at this frequency. Since the correction factors are large, the engineering method would give large errors and the hybrid method would produce more accurate results. Lastly, the corrections depend strongly on  $\Delta y$  and would not have been predicted well by a 2D model. This observation justifies choosing the more expensive 2.5D BEM instead of the more economical 2D BEM to calculate the correction factors.

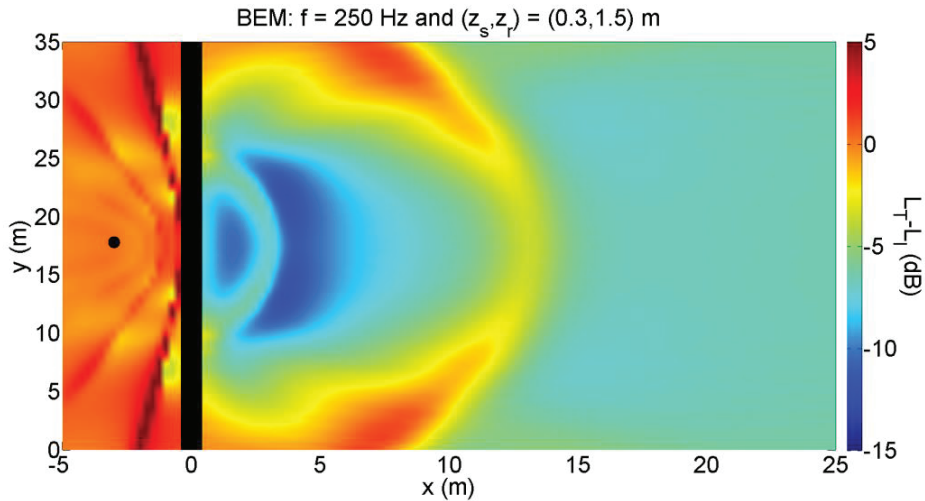


Figure 6 – A 2.5D BEM calculation of the attenuation of the T-top

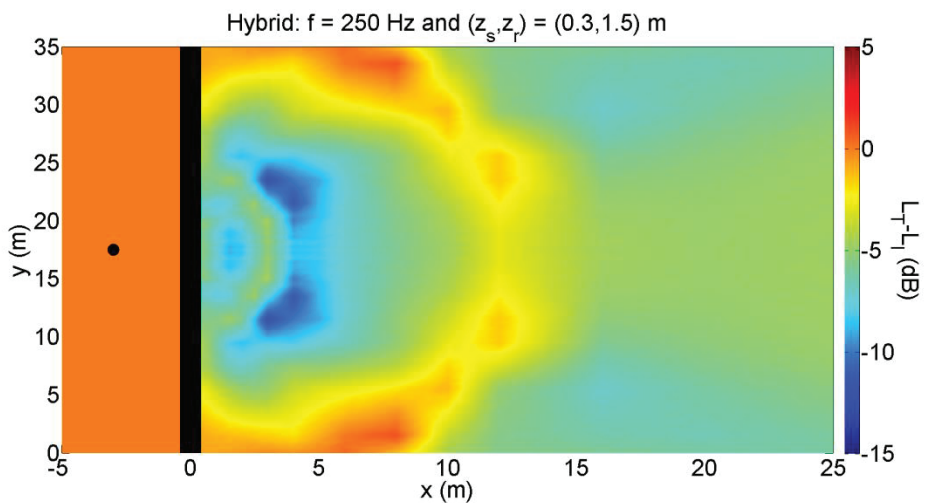


Figure 7 – A hybrid calculation of the attenuation of the T-top

There are two reasons why Figure 6 and Figure 7 do not look identical. First, on the source side of the barrier the model assumes that  $A_{complex}$  is zero, which explains why the level is constant on the left-hand side of the barrier. This simplification is generally not problematic since the source side is typically quite loud and the barrier is not generally designed to reduce the noise on the source side but rather on the back side. Thus, a correction on the source side is usually unnecessary.

Second, on the right-hand side of the barrier the differences stem from the coarse spacing of the points in the input file. Recall from Section 2.2 that the grid points are concentrated close to the barrier and grow further apart moving away from the barrier. Figure 7 substantiates this choice and illustrates that even with a limited amount of input data, the general pattern is still represented. Nevertheless, since changes occur on the order of a wavelength, the current spacing may not be sufficient to represent higher frequencies as accurately. This paper only considers low frequencies (250 Hz third-octave), so this issue is not addressed here.

### 3.2 T-barrier with buildings

Next, consider a T-barrier in a complex scene (see Figure 8). Everything is the same as in the previous case except there are two buildings where the bottom building is 6 m tall and the top building is 8 m tall. Figure 8 gives  $A_{complex}$  using 3D BEM and Figure 9 gives  $A_{complex}$  using the hybrid method. This case demonstrates the improvement that the hybrid method makes compared to the engineering method alone and the limitations of the hybrid method.

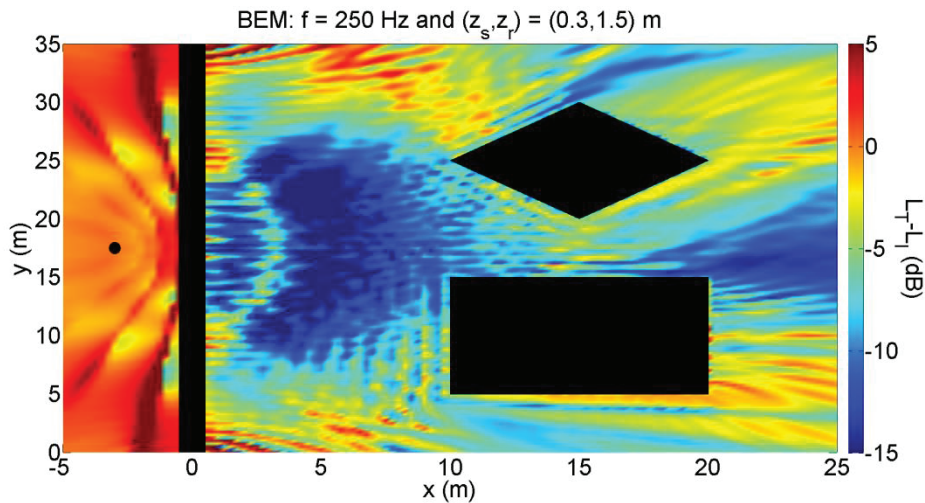


Figure 8 – A 3D BEM calculation of the attenuation of the T-top in a complex setting

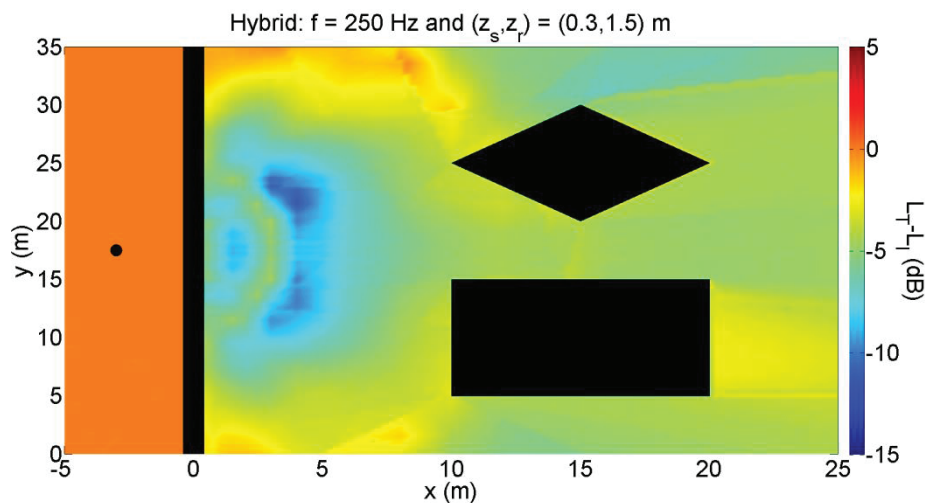


Figure 9 – A hybrid calculation of the attenuation of the T-top in a complex setting

Qualitatively, the hybrid method does quite well. The overall pattern is similar especially between the barrier and the buildings. In addition, the correction is generally in the correct direction, so the correction is providing an improvement over the engineering method.

However, there are many large differences. Some differences are expected when the reference method takes days to compute and the hybrid method only takes seconds. Moreover, some of these differences occur because the two methods are not quite modeling the same physical case. 3D BEM is modeling a finite length barrier that is 35 m long and the hybrid method is modeling an infinitely long barrier. Thus, the sound that diffracts around the ends of the barrier is modeled in BEM (Figure 10, which plots the *total* pressure for the T-barrier) but not in the hybrid method. Another important difference stems from how the engineering method sums the contributions from each of the paths. The engineering method sums the path contributions without phase information, so destructive interference is not possible, but BEM includes this phase information. Contrasting the BEM plots, the areas that have lower levels in Figure 8 than in Figure 6 are likely places of the destructive interference.

Remember, the main goal of the hybrid method is to give a reasonable approximation for cases that are slightly more complex than what the current engineering methods can handle at little extra cost. This case is fairly small (30 m x 35 m) with only one complex object and two buildings at a low frequency (250 Hz third-octave) to enable 3D BEM to model the same case. This mesh size and frequency are nearing the limits of ordinary 3D BEM, so potentially the hybrid method is particularly useful for larger scenes (typically multiple city blocks) at higher frequencies (typically up to 5 kHz).

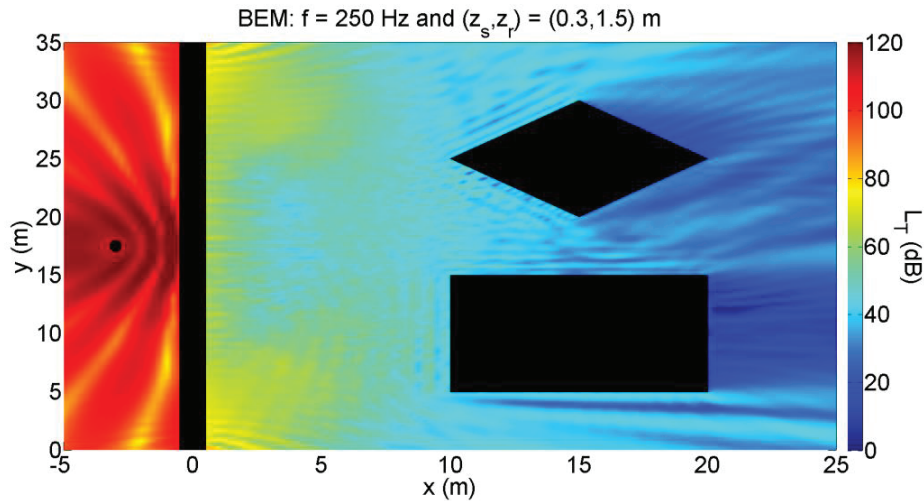


Figure 10 – A 3D BEM calculation of the total pressure of a T-barrier in a complex setting

### 3.3 Computational Performance

Three computations increase in time with a larger number of source/receiver pairs: computing  $A_{complex}$  with BEM, loading the input file, and searching for a point in the data table. All of the other computations are constant in time and negligibly increase the total computation time. The calculation time for BEM is much longer than for the engineering method (hours compared to seconds). However, this calculation is only performed once per complex object because engineering methods assume that the sources of attenuation are mostly independent. This assumption is not always true, but it drastically simplifies the problem and usually provides reasonable results. Thus, a user of this method could have a library of these corrections all precomputed so that the computation time of this portion becomes unimportant. Furthermore, these corrections could be shared among users.

In addition, the hybrid method is much more computationally efficient than only using 3D BEM. The hybrid method only discretizes the perimeter of the barrier's cross section whereas 3D BEM would need to mesh all of the surfaces of the entire scene. Therefore, the hybrid method is much less expensive than 3D BEM.

Next, loading the data file also increases the computation time and the required memory. The input file must be loaded each time the user wants to run computations but does not need to be loaded for each path in the engineering method. The cost for both memory and time increase linearly with the number of source/receiver pairs in the input file (see Table 2). In the input file, each line has the location of the source and receiver and twenty-one third-octave (50 Hz – 5 kHz) corrections. Even for large input files (up to 1 GB), load times are not very long (about 40 s).

| Lines | File Size | Load Time |
|-------|-----------|-----------|
| 243   | 57 KB     | 2 ms      |
| 3.1 k | 720 KB    | 25 ms     |
| 59 k  | 13 MB     | 460 ms    |
| 1.4 M | 320 MB    | 11 s      |
| 5.2 M | 1.1 GB    | 40 s      |

Table 2 – The additional computation time of the hybrid method depends linearly on the size of the input file

As the number of source/receiver pairs grows, the search time to find one pair also increases. Currently, a kd-tree finds the points in a time that is proportional to  $\log_2 N$  where  $N$  is the number of source/receiver pairs. The additional computation time, which is less than  $10 \mu\text{s}/\text{path}$  for files with up to five million lines, is negligible compared to the computation time of the engineering method, which is about  $1 \text{ ms}/\text{path}$  or more depending on the complexity of the scene.

#### 4. CONCLUSIONS

This paper outlines an efficient procedure to incorporate the impact of complex geometries in urban environments into an engineering method. The hybrid method utilizes a reference method to calculate the attenuation of the complex object compared to a reference object. Interpolating these results at the appropriate source and receiver positions yields the attenuation term for the corresponding path. The results shown above demonstrate that this hybrid method improves the accuracy of the engineering methods at little extra cost.

There are still many potential ways for this hybrid method to be improved. The most important advancement is to determine how to get the greatest accuracy with a limited number of data points. Currently, the method uses a non-uniform grid because it is easy to implement and makes searching for points very efficient. However, another data structure (e.g. an adaptive mesh) may provide better accuracy but would likely have a larger computational burden. In addition, since this paper only looks at low frequencies (250 Hz third-octave) in a small, simple scene compared to a city, future research should consider higher frequencies and larger, more complicated scenes. Lastly, the implementation of multiple diffracting objects needs to be studied in further detail and changed accordingly.

#### ACKNOWLEDGEMENTS

This research is funded by the Building Science and Technology Center (in French: Centre Scientifique et Technique du Bâtiment; CSTB).

#### REFERENCES

1. World Health Organization Regional Office for Europe. Guidelines for community noise. 1999.
2. World Health Organization Regional Office for Europe. Night noise guidelines for Europe. 2009.
3. World Health Organization Regional Office for Europe. Burden of disease from environmental noise: Quantification of healthy life years lost in Europe. 2011.
4. World Health Organization Regional Office for Europe. Methodological guidance for estimating the burden of disease from environmental noise. 2012.
5. Directive 2002/49/EC of the European parliament and the council of 25 June 2002 relating to the assessment and management of environmental noise. 2002.
6. ISO 6913-2: Acoustics - Attenuation of sound during propagation outdoors - Part 2: General method of calculation. 1996.
7. Sétra. Road noise prediction: Part 2 - Noise propagation computation method including meteorological effects (NMPB 2008). 2009.
8. Dutilleul G, Defrance J, Ecotière D, Gauvreau B, Bérengier M, Besnard F, et al. NMPB-routes-2008: The revision of the french method for road traffic noise prediction. *Acta Acust united with Acust.* 2010;96(3):452–62.
9. DELTA. Nord2000. Comprehensive Outdoor Sound Propagation Model. Part 1: Propagation in an Atmosphere without Significant Refraction. 2006.
10. DELTA. Nord2000. Comprehensive Outdoor Sound Propagation Model. Part 2: Propagation in an Atmosphere with Refraction. 2006.
11. European Commission-Joint Research Centre. Common Noise Assessment Methods in Europe (CNOSSOS-EU). 2012.
12. Van Maercke D, Defrance J. Development of an analytical model for outdoor sound propagation within the harmonoise project. *Acta Acust united with Acust.* 2007;93(2):201–12.
13. Salomons E, Van Maercke D, Defrance J, De Roo F. The Harmonoise sound propagation model. *Acta Acust united with Acust.* 2011;97(1):62–74.
14. Farina A. Validation of the pyramid tracing algorithm for sound propagation outdoors: Comparison with experimental measurements and with the ISO-DIS 9613 standards. *Adv Eng Softw.* 2000;31(4):241–50.
15. Wang H, Yu Z, Cai M. The 3D Attenuation Calculation of Traffic Noise among Building Groups by Using Beam Tracing Method. *Procedia - Soc Behav Sci.* Elsevier B.V.; 2013 Nov;96:1929–37.
16. Bradley JS. A Study of Traffic Noise Attenuation Around Buildings. *Acta Acust united with Acust.* 1977;38(4):247–52.
17. Hewett DP. High frequency sound propagation in a network of interconnecting streets. *J Sound Vib.* Elsevier; 2012 Dec;331(25):5537–61.
18. Kang J. Sound propagation in street canyons: Comparison between diffusely and geometrically

- reflecting boundaries. *J Acoust Soc Am*. 2000;107(3):1394–404.
19. Kang J. Numerical modeling of the sound fields in urban squares. *J Acoust Soc Am*. 2005;117(6):3695–706.
  20. Picaut J, Simon L, Hardy J. Sound field modeling in streets with a diffusion equation. *J Acoust Soc Am*. 1999;106(5):2638–45.
  21. Picaut J. Numerical modeling of urban sound fields by a diffusion process. *Appl Acoust*. 2002 Sep;63(9):965–91.
  22. Pasareanu S. Energy-based method for near real-time modeling of sound field in complex urban environments. *J Acoust Soc Am*. 2012;132(6):3647–58.
  23. Hothersall D. Efficiency of single noise barriers. *J Sound Vib*. 1991;146(2):303–22.
  24. Jean P. A variational approach for the study of outdoor sound propagation and application to railway noise. *J Sound Vib*. 1998;212(2):275–94.
  25. Defrance J, Jean P. Integration of the efficiency of noise barrier caps in a 3D ray tracing method. Case of a T-shaped diffracting device. *Appl Acoust*. 2003 Aug;64(8):765–80.
  26. Baulac M, Defrance J, Jean P, Minard F. Efficiency of noise protections in urban areas: Predictions and scale model measurements. *Acta Acust united with Acust*. 2006;92(4):530–9.
  27. Fan R, Su Z, Cheng L. Modeling, analysis, and validation of an active T-shaped noise barrier. *J Acoust Soc Am*. 2013 Sep;134(3):1990–2003.
  28. Ogren M. Road Traffic Noise Propagation between Two Dimensional City Canyons using an Equivalent Sources Approach. *Acta Acust united with Acust*. 2004;90:293–300.
  29. Hornikx M, Forssén J. Noise abatement schemes for shielded canyons. *Appl Acoust*. Elsevier Ltd; 2009 Feb;70(2):267–83.
  30. Mehra R, Raghuvanshi N, Antani L, Chandak A, Curtis S, Manocha D. Wave-based sound propagation in large open scenes using an equivalent source formulation. *ACM Trans Graph*. 2013;32(2):19:1–13.
  31. Van Renterghem T, Botteldooren D. The importance of roof shape for road traffic noise shielding in the urban environment. *J Sound Vib*. Elsevier; 2010;329(9):1422–34.
  32. Van Renterghem T, Hornikx M, Forssen J, Botteldooren D. The potential of building envelope greening to achieve quietness. *Build Environ*. Elsevier Ltd; 2013;61:34–44.
  33. Mehra R, Raghuvanshi N, Chandak A, Albert DG, Wilson DK, Manocha D. Acoustic pulse propagation in an urban environment using a three-dimensional numerical simulation. *J Acoust Soc Am*. 2014 Jun;135(6):3231–42.
  34. Oshima T, Ishizuka T, Kamijo T. Three-dimensional urban acoustic simulations and scale-model measurements over real-life topography. *J Acoust Soc Am*. 2014 Jun;135(6):EL324–30.
  35. Hofmann J, Heutschi K. Simulation of outdoor sound propagation with a transmission line matrix method. *Appl Acoust*. 2007 Feb;68(2):158–72.
  36. Guillaume G, Picaut J, Dutilleux G, Gauvreau B. Time-domain impedance formulation for transmission line matrix modelling of outdoor sound propagation. *J Sound Vib*. 2011 Dec;330(26):6467–81.
  37. Guillaume G, Aumond P, Gauvreau B, Dutilleux G. Application of the transmission line matrix method for outdoor sound propagation modelling – Part 1: Model presentation and evaluation. *Appl Acoust*. 2014 Feb;76:113–8.
  38. Jean P. Coupling Geometrical and Integral Methods for Indoor and Outdoor Sound Propagation Validation Examples. *Acta Acust united with Acust*. 2001;87:236–46.
  39. Premat E, Defrance J, Priour M, Aballea F. Coupling BEM and GFPE for complex outdoor sound propagation. *Proceedings of Euronoise-Naples*. 2003. p. 1–6.
  40. Van Renterghem T, Salomons E, Botteldooren D. Parameter study of sound propagation between city canyons with a coupled FDTD-PE model. *Appl Acoust*. 2006 Jun;67(6):487–510.
  41. Defrance J, Salomons E, Noordhoek I, Heimann D, Plovsing B, Watts G, et al. Outdoor sound propagation reference model developed in the European harmonoise project. *Acta Acust united with Acust*. 2007;93(2):213–27.
  42. Yeh H, Mehra R, Ren Z, Antani L, Manocha D, Lin M. Wave-ray coupling for interactive sound propagation in large complex scenes. *ACM Trans Graph*. 2013 Nov 1;32(6):165:1–11.
  43. Oldham DJ, Egan CA. A parametric investigation of the performance of T-profiled highway noise barriers and the identification of a potential predictive approach. *Appl Acoust*. Elsevier Ltd; 2011;72(11):803–13.
  44. Kasess CH, Kreuzer W, Waubke H. Deriving correction functions to model the efficiency of noise

barriers with complex shapes using boundary element simulations. *Appl Acoust.* Elsevier Ltd; 2016;102:88–99.